Journal of Power Sources 227 (2013) 153–160

Contents lists available at SciVerse ScienceDirect

Journal of Power Sources

journal homepage: www.elsevier.com/locate/jpowsour

Synthesis of electro-deposited ordered mesoporous RuO_x using lyotropic liquid crystal and application toward micro-supercapacitors

Sho Makino [a], Yusuke Yamauchi [b,c,*], Wataru Sugimoto [a,**]

[a] Faculty of Textile Science and Technology, Shinshu University, 3-15-1 Tokida, Ueda, Nagano 386-8567, Japan
[b] World Premier International Research Center for Materials Nanoarchitectonics, National Institute for Materials Science, Namiki 1-1, Tsukuba, Ibaraki 305-0044, Japan
[c] Precursory Research for Embryonic Science and Technology, Japan Science and Technology Agency, Kawaguchi, Saitama 332-0012, Japan

HIGHLIGHTS

- Ordered mesoporous Ru was electrochemically prepared via liquid crystal templating.
- Electro-oxidation resulted in ordered mesoporous RuO_x with ~400 F g^{-1}.
- Deposition of mesoporous Ru on μ-electrodes with 5 μm gap was achieved.
- RuO_x micro-supercapacitor had specific capacitance of 12.6 mF cm^{-2}.
- RuO_x micro-supercapacitor had specific energy of 12.5 Wh kg^{-1}.

GRAPHICAL ABSTRACT

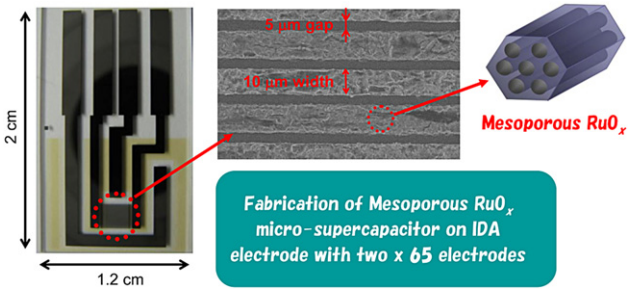

ARTICLE INFO

Article history:
Received 10 November 2012
Accepted 12 November 2012
Available online 23 November 2012

Keywords:
Mesoporous materials
Ruthenium oxide
Lyotropic liquid crystal
Supramolecular templating
Electrochemical capacitor
Micro-supercapacitor

ABSTRACT

Synthesis of ordered mesoporous RuO_x electrodes was conducted by electro-deposition using a lyotropic liquid crystal template method with Ti substrates and subsequent electro-oxidation. The obtained ordered mesoporous Ru metal was characterized by XRD, TEM and electrochemical measurements in 0.5 M H_2SO_4. After electro-oxidation by potential cycling, the ordered mesoporous RuO_x afforded specific capacitance of ~400 F (g-Ru)$^{-1}$. A micro-supercapacitor with ordered mesoporous RuO_x was fabricated by controlled electro-deposition of ordered mesoporous RuO_x on an inter-digitated array electrode (IDA; 10 μm electrode width, 5 μm gap and 65 × 2 electrodes). This micro-supercapacitor exhibited good capacitive property with maximum specific capacitance of 12.6 mF cm^{-2} and specific energy of 12.5 Wh (kg-Ru)$^{-1}$ based on the mass of the deposited material.

1. Introduction

The recent surge for sophisticated portable electronics and wireless networks for smart environments has proven the necessity of sufficiently small-sized compact energy storage devices (micro-supercapacitors). The challenge is to integrate the active material on electrodes as close as possible to the electronic circuit (on chip). For such micro-devices, MEMS technology is the most favorable choice of fabrication as exemplified by smart dust, μ-TAS

* Corresponding author. World Premier International Research Center for Materials Nanoarchitectonics, National Institute for Materials Science, Namiki 1-1, Tsukuba, Ibaraki 305-0044, Japan. Tel.: +81 29 860 4635.
** Corresponding author. Tel.: +81 268 21 5455; fax: +81 268 21 5452.
E-mail addresses: Yamauchi.Yusuke@nims.go.jp (Y. Yamauchi), wsugi@shinshu-u.ac.jp (W. Sugimoto).

0378-7753/$ – see front matter © 2012 Elsevier B.V. All rights reserved.
http://dx.doi.org/10.1016/j.jpowsour.2012.11.032

[1,2] and μ-DMFC [3]. Micro-supercapacitor should be suitable as an auxiliary power source and for load-leveling, owing to the high power density and long-cycle life [4]. Supercapacitors (electrochemical capacitors) are energy storage devices that utilize the electric double layer formed near the electrode surface sometimes accompanied by fast reversible surface redox reactions, thus allowing fast and non-destructive energy harvesting with virtually no need for thermal management. Conducting polymers such as polypyrrole [5–8] and carbonaceous material [9–13] have been used as active materials for micro-supercapacitor. The fabrication of micro-supercapacitor in most cases relies on wet-chemical methods, such as photolithographic processes and ink-jet printing techniques since it is necessary to deposit a small amount of active material onto a micro-size region.

In aqueous electrolytes RuO_2-based materials show extremely large specific capacitance [14]. Due to the lack of abundance of the precious metal, such high performance material should find use in applications where the deposited mass is quite low, i.e. micro-supercapacitors. Micro-supercapacitor with 0.5 mm × 2 mm × 2 electrode (20 μm gap) made by deposition of $RuO_2 \cdot nH_2O$ using direct-laser printing method onto conducting substrate has been reported to show high energy density of 9 mW g^{-1} [15]. Fabrication of micro-supercapacitor composed of a pair of 10 electrodes with 40 μm electrode width and 40 μm gap by inkjet-printing of activated carbon has also been achieved [9]. Electrochemical deposition processes have been successfully applied to deposit conducting polymers such as polypyrrole directly onto electrodes [5–8]. Regardless of the fabrication techniques, the common challenge is to deposit porous material on micro-sized substrates without shorting the positive and negative electrodes.

In this study, we have attempted to deposit ordered mesoporous RuO_x onto a commercial inter-digitated array (IDA) electrode consisting of a pair of 65 electrodes with 10 μm electrode width, 5 μm gap. As far as the authors are aware of, the electrode width and gap of the micro-electrode used in this study are the smallest ever to be applied for micro-supercapacitor applications. We have chosen to apply a combination of electro-deposition (for precisely controlled deposition), lyotropic liquid crystal templating (for producing a Ru metal with an ordered mesostructure), and electro-oxidation (for gentle oxidation of deposited Ru to RuO_x). Ordered mesoporous Pt [16–19], Ni [20,21], Ru [22] and $Ni(OH)_2$ [23,24] have been prepared by supermolecular assembly of surfactants as template. We have also shown that ordered mesoporous metallic Ru can be prepared by chemical reduction of Ru^{n+} introduced into hydrophilic region of non-ionic surfactant Brij 56 [25]. Furthermore, ordered mesoporous Ru metal was successfully converted to RuO_x by electro-oxidation while maintaining its mesoporous structure [25].

First the details of the synthesis and electrochemical capacitor behavior of ordered mesoporous RuO_x onto Ti substrate with 1.5 cm × 1.5 cm by electro-deposition and electro-oxidation are illustrated. Next, the fabrication of a micro-supercapacitor using commercial IDA electrode is demonstrated. Ordered mesoporous Ru metal was electro-deposited directly onto IDA electrode by using a bi-potentiostat with four-electrode system to separately control the electro-deposition behavior of two working electrodes on the IDA electrode. After electro-oxidation, the electrochemical capacitive property of the obtained mesoporous RuO_x micro-supercapacitor was evaluated by cyclic voltammetry and constant current charge/discharge measurement.

2. Experimental

Hexagonal lyotropic liquid crystal with Ru^{n+} precursor in hydrophilic region was prepared by mixing $RuCl_3$, non-ionic surfactant Brij 56 ($C_{16}H_{33}(OCH_2CH_2)_nOH$, $n \sim 10$) and H_2O in the predetermined ratio (Brij 56:$RuCl_3$:H_2O = 7.5:0.5:7.0 in mass). This well-mixed lyotropic liquid crystal was used as the electro-deposition bath. The electro-deposition process was conducted in a three-electrode system consisting of a titanium plate working electrode (1.5 cm × 1.5 cm), a platinum mesh counter electrode and a Ag/AgCl/KCl (sat.) reference electrode. Ordered mesoporous Ru metal was electro-deposited onto Ti plate at constant potential (−0.2 V vs. Ag/AgCl for 8 h, −0.3, −0.4, −0.5, −0.6 V vs. Ag/AgCl for 1 h). After electro-deposition, the sample was carefully washed sequentially with ethanol, acetone and ultrapure water to remove the Brij 56 template and any un-reacted $RuCl_3$. Ordered structure of electro-deposited mesoporous Ru metal was characterized by X-ray diffraction (XRD, Rigaku RINT-Ultima/S2K with monochromated CuKα radiation) and transmission electron microscopy (TEM, JEOL JEM-2010).

Electrochemical measurements were carried out using a beaker-type electrochemical cell composed of a Pt mesh counter electrode and a Ag/AgCl/KCl (sat.) reference electrode connected with salt bridge. A Luggin capillary faced the working electrode at a distance of 2 mm. Electrode potentials will be referred to the reversible hydrogen electrode (RHE) potential scale. In order to evaluate the electrochemical active surface area of the electro-deposited mesoporous Ru metal, CO stripping voltammetry was conducted by electro-oxidation of pre-adsorbed carbon monoxide (CO_{ad}) in 0.5 M H_2SO_4 at a scan rate of 10 mV s^{-1}. The amount of CO_{ad} was calculated by integration of the CO_{ad} stripping peak, corrected for the electrical double layer capacitance, assuming a monolayer of linearly adsorbed CO on the metallic Ru surface and the Coulombic charge necessary for oxidation as 420 μC cm^{-2}. Electrochemical oxidation was carried out to convert from Ru metal to RuO_x by potential cycling between 0.2 and 1.2 V vs. RHE at a scan rate of 50 mV s^{-1} for 500 cycles. Then the capacitive behavior of electro-oxidized mesoporous RuO_x was estimated by cyclic voltammetry in 0.5 M H_2SO_4 electrolyte and the specific capacitance was calculated by averaging the anodic and cathodic charge from the cyclic voltammograms.

A commercialized inter-digitated array (IDA) electrode (BAS Inc., Japan) was used as a micro-supercapacitor substrate. Electro-deposition process of mesoporous Ru metal onto IDA electrode was performed by using a bi-potentiostat. The IDA electrode is composed of two 65 carbon electrodes (2 mm long × 10 μm width and 5 μm gap, 1.3 mm^2 per electrode) and a carbon counter electrode. A Ag/AgCl/KCl (sat.) electrode was used as the reference electrode. First, the potential of electrode 1 was set to −0.3 V vs. Ag/AgCl while applying 1.0 V vs. Ag/AgCl to electrode 2 for 15 min. This allowed deposition of mesoporous Ru metal on electrode 1 while preventing unnecessary deposition of Ru metal onto electrode 2. Then, the potentials of the two working electrodes were reversed to electro-deposit mesoporous Ru metal onto electrode 2. This sequence was repeated 3 times. After electro-deposition, the electrode was thoroughly washed with ethanol and ultrapure water. Finally, mesoporous Ru/IDA was electro-oxidized by potential cycling between 0.2 and 1.2 V vs. RHE at a scan rate of 50 mV s^{-1} for 500 cycles in 0.5 M H_2SO_4 to obtain mesoporous RuO_x/IDA. The capacitive behavior was evaluated by cyclic voltammetry for the three-electrode system and by constant current charge/discharge measurements in the case of two-electrode configuration in 0.5 M H_2SO_4.

3. Results and discussions

3.1. Electrochemical deposition of mesoporous Ru metal and capacitive behavior of electro-oxidized mesoporous RuO_x

The low angle XRD patterns of electro-deposited mesoporous Ru metal prepared at different deposition potentials (E_{ED}) are

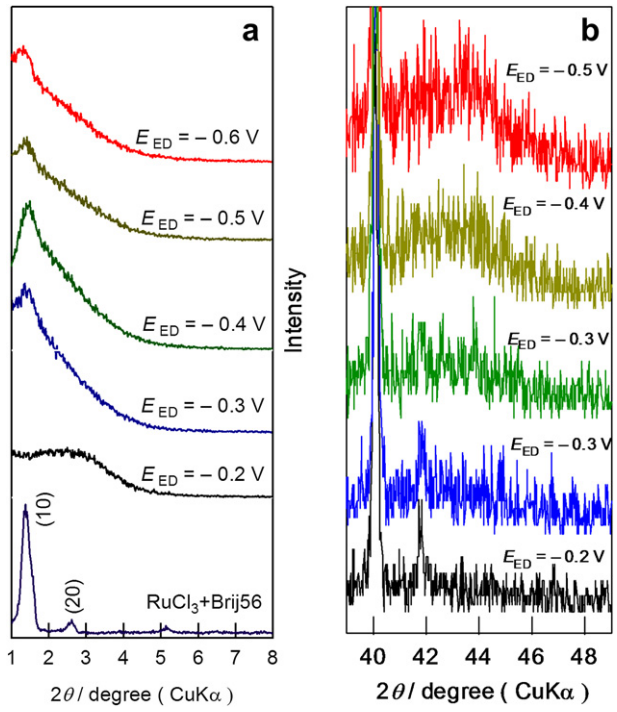

Fig. 1. (a) Low and (b) high angle XRD patterns of thin film products obtained at various electro-deposition potentials, E_{ED}. The XRD pattern of the mixture of the precursor before electro-deposition is shown in (a) as a reference.

shown in Fig. 1a. The lyotropic liquid crystal phase containing $RuCl_3$ precursor (sample before electro-deposition) is also shown as a reference. The low angle XRD peaks of the sample before applying any potential can be indexed based on a hexagonal crystal structure, indicating ordered arrangement of micelle in lyotropic liquid crystal phase. After electro-deposition, a broad XRD peak centered at $d = 5.8$ nm was observed for $E_{ED} \leq -0.3$ V vs. Ag/AgCl. The d values after electro-deposition agreed with d_{10} value of lyotropic liquid crystal phase before deposition ($d_{10} = 5.9$ nm), suggesting that the ordered porous structure of the parent lyotropic liquid crystal phase is preserved in the electro-deposited film. The d_{10} value of 5.8 nm corresponds to a pore-to-pore distance of 6.7 nm. These results are in agreement with that of chemically reduced mesoporous Ru metal [25]. At $E_{ED} = -0.2$ V vs. Ag/AgCl the low angle XRD peak was severely broadened and observed at higher diffraction angle, suggesting a disordered meso-structure.

Evidence of reduction to Ru metal was obtained from the high angle XRD patterns (Fig. 1b). A weak, broad peak was observed near $2\theta = 41°–44°$ at low E_{ED}, which correspond to the (002) and (101) diffraction peaks for Ru metal.

The TEM images of various electro-deposited mesoporous Ru metal films are shown in Fig. 2. The samples were mechanically scraped off from Ti substrate for the TEM observations. Ordered mesoporous array was observed for $E_{ED} \leq -0.3$ V vs. Ag/AgCl. The one dimensional tunnel-like pores observed in Fig. 2c reflect the structure of the hexagonal phase. The distance observed in the TEM image ($\sim$6 nm) closely matches the $d_{10} = 5.9$ nm calculated from XRD pattern. The mesoporous structure of electro-deposited film at −0.6 V vs. Ag/AgCl was hexagonal (Fig. 2e). The pore-to-pore distance of 7–7.5 nm observed for the film electro-deposited at −0.6 V vs. Ag/AgCl is consistent with the estimated value obtained from the XRD pattern (6.7 nm). The TEM images also reveal that the meso-structures have a wall thickness of about 3 nm. The TEM images of the sample obtained at $E_{ED} = -0.2$ V vs. Ag/Ag/Cl (Fig. 2a) showed no evidence of ordered structure, which is in agreement with the XRD data. Based on the results from XRD measurements and TEM observations, it is concluded that ordered mesoporous Ru

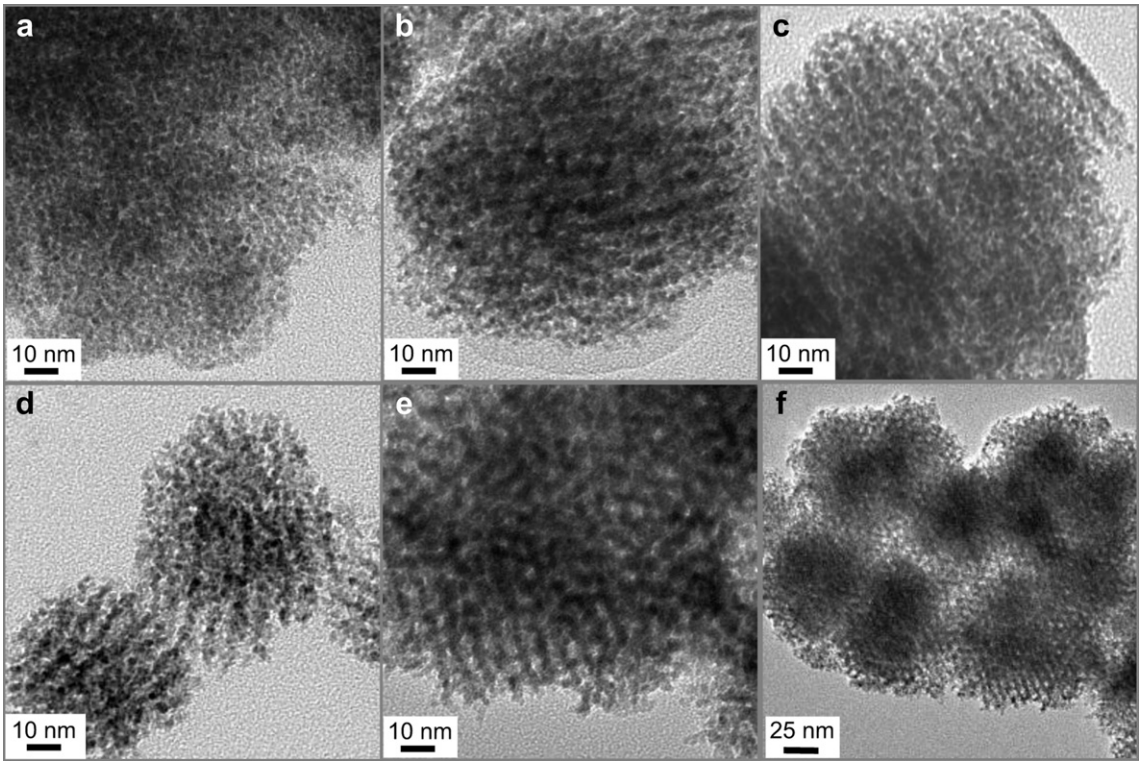

Fig. 2. TEM images of mesoporous Ru metal electro-deposited at (a) −0.2, (b) −0.3, (c) −0.4, (d) −0.5, and (e, f) −0.6 V vs. Ag/AgCl.

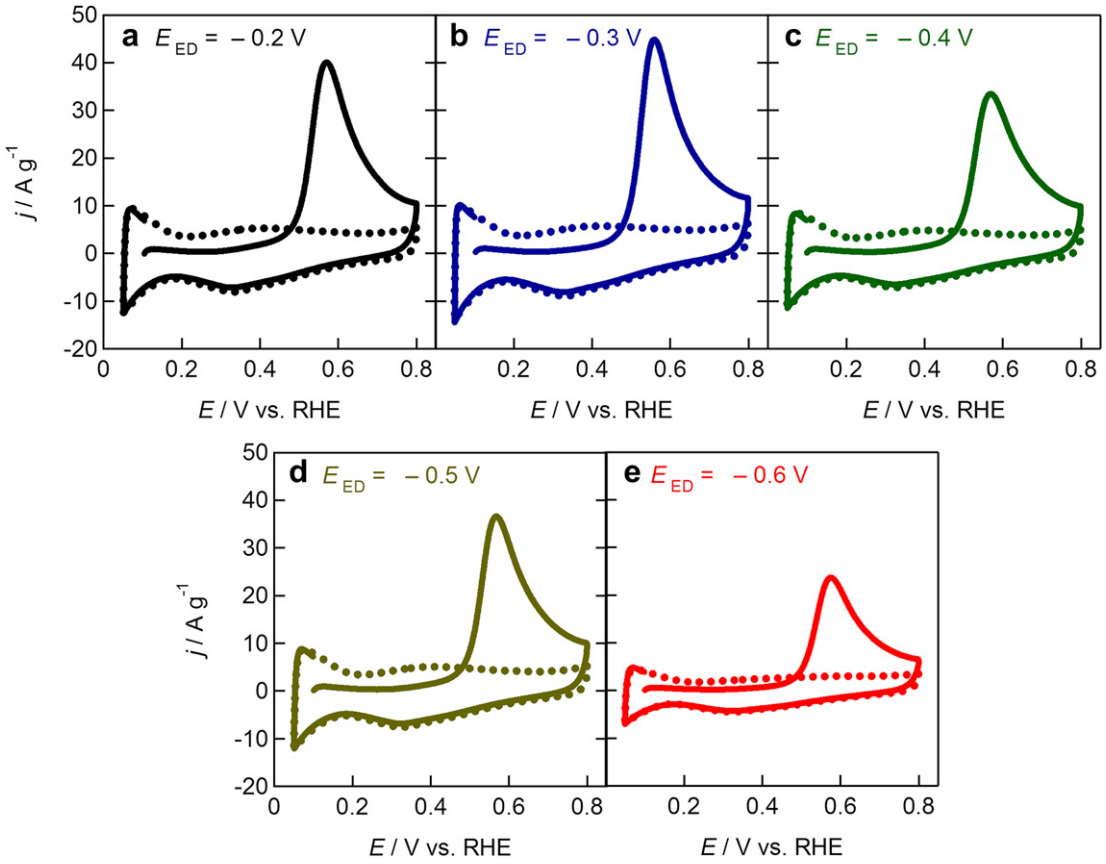

Fig. 3. CO-stripping voltammograms of mesoporous Ru metal at 10 mV s^{-1} in 0.5 M H_2SO_4 obtained by electro-deposition at (a) −0.2, (b) −0.3, (c) −0.4, (d) −0.5, and (e) −0.6 V vs. Ag/AgCl.

metal film was successfully electro-deposited when $E_{ED} \leq -0.3$ V vs. Ag/AgCl.

The electrochemical active surface area of mesoporous Ru metal was evaluated by CO-stripping method. CO-stripping voltammograms of the products obtained at various E_{ED} are shown in Fig. 3. The voltammograms are similar in shape to carbon supported Ru metal [26]. The electrochemically active surface areas ranged between 70 and 130 $m^2\ g^{-1}$ (Table 1).

Ordered mesoporous Ru metal was electro-oxidized to convert to mesoporous RuO_x by sweeping the potential between 0.2 and 1.2 V vs. RHE for 500 cycles at 50 mV s^{-1} (Fig. S1). A typical TEM image of the electro-oxidized product is shown in Fig. 4. The ordered mesoporous structure is sustained after the electro-oxidation process. Cyclic voltammograms of ordered mesoporous RuO_x after electro-oxidation are shown in Fig. 5. The cyclic voltammograms exhibited rectangular shape with a broad redox peak at 0.7 V vs. RHE, typical of ideal capacitive behavior including some contribution from pseudo-capacitance. Ordered mesoporous RuO_x exhibited high

Table 1
Electrochemically active surface area of mesoporous Ru/Ti and specific capacitance of mesoporous RuO_x/Ti.

E_{ED}/V vs. Ag/AgCl	Electrochemically active surface area/$m^2\ g^{-1}$	Specific capacitance/F $(g\text{-}Ru)^{-1}$
−0.20	130	450
−0.30	130	380
−0.40	110	370
−0.50	120	410
−0.60	70	340

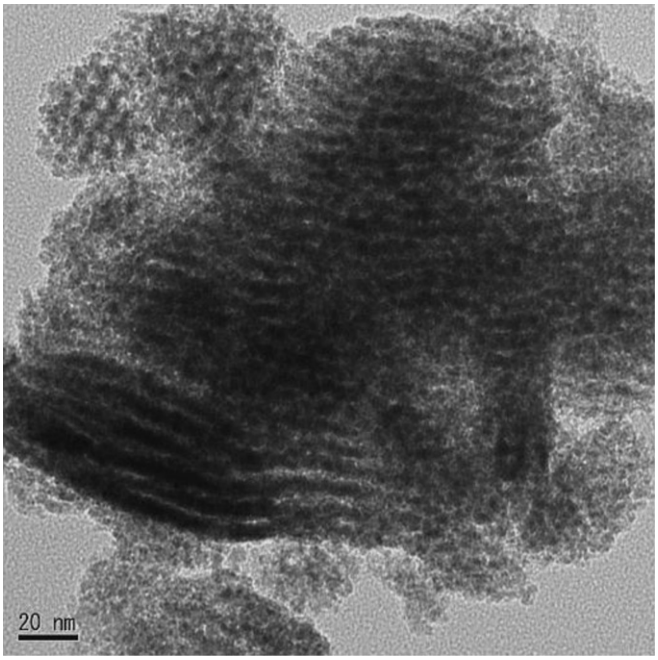

Fig. 4. TEM image of ordered mesoporous RuO_x electro-deposited at −0.6 V vs. Ag/AgCl and subsequently electro-oxidized.

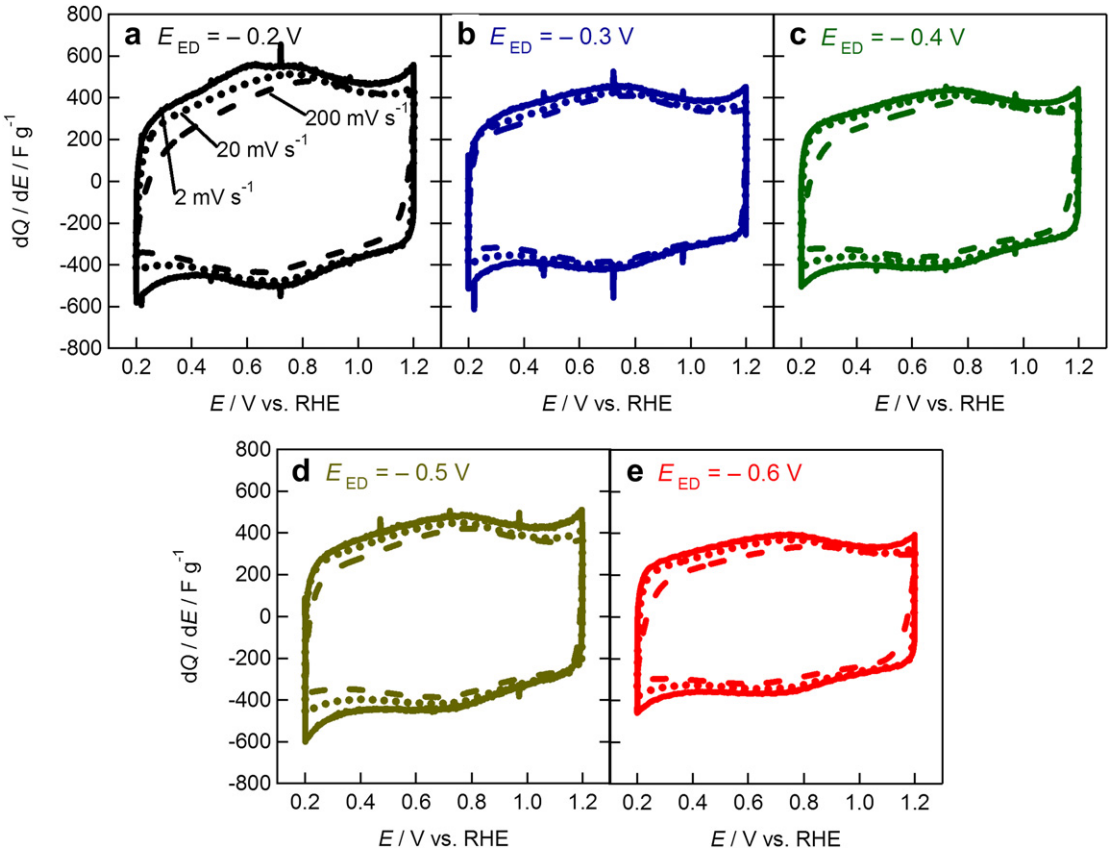

Fig. 5. Cyclic voltammograms of mesoporous RuO_x after electro-oxidation of mesoporous Ru metal obtained by electro-deposition at (a) −0.2, (b) −0.3, (c) −0.4, (d) −0.5, and (e) −0.6 V vs. Ag/AgCl. Electrolyte: 0.5 M H_2SO_4, scan rate 2 (line), 20 (dotted line), 200 (broken line) mV s^{-1}.

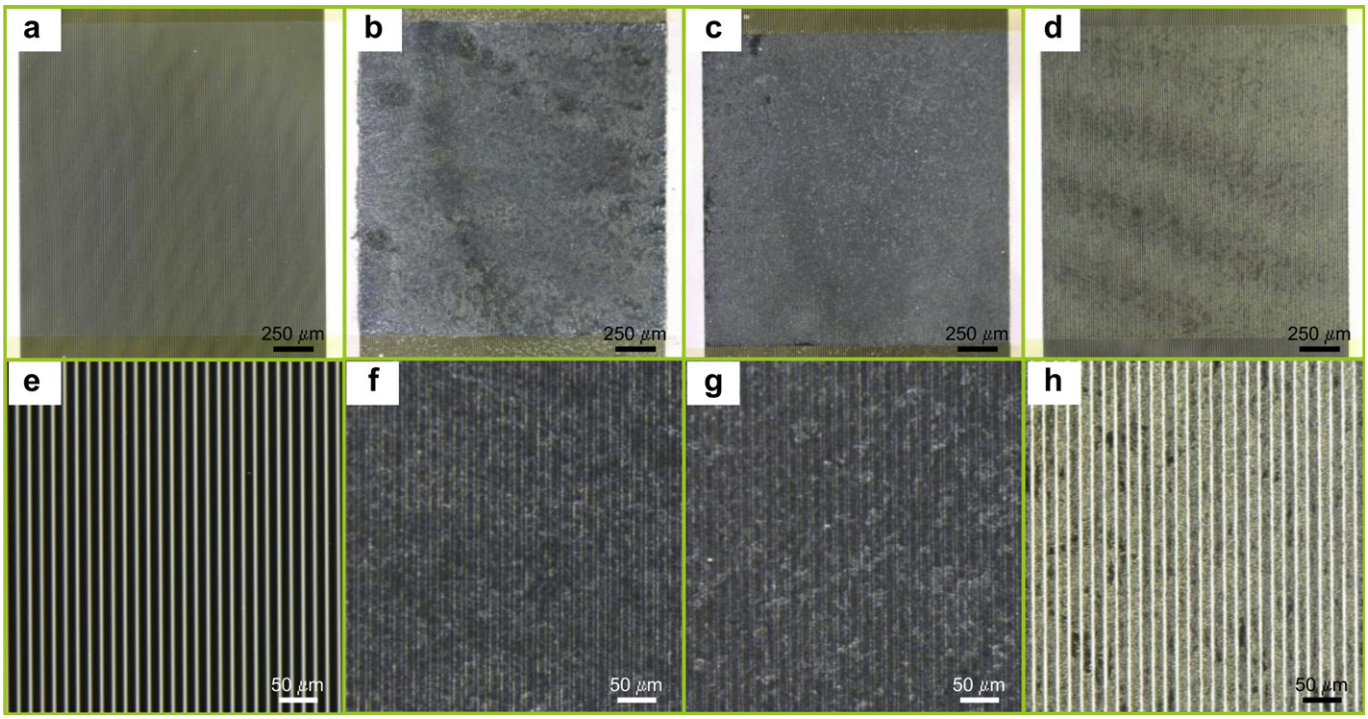

Fig. 6. Optical microscopic images of overall (a–d) and magnified view (e–h) for IDA electrode. (a,e) Before electro-deposition (as-received IDA electrode). After electro-deposition of mesoporous Ru metal onto IDA electrode by (b,f) electro-depositing both electrodes at once (Scheme 1a), (c,g) sequential electro-deposition onto one electrode at a time (Scheme 1b), and (d,h) bi-potentiostatic electro-deposition onto one electrode at a time (Scheme 1c).

specific capacitance of ~400 F (g-Ru)$^{-1}$ (Table 1). The specific capacitance in this study is smaller than that of $RuO_2 \cdot nH_2O$ prepared by sol–gel method [14] probably due to the larger primary particle with about 3 nm diameter and possible incomplete oxidation. Under the electro-oxidation conditions applied in this study, only surface and/or near surface layers may have been oxidized.

3.2. Micro-supercapacitor properties of inter-digitated array electrode modified with electro-deposited mesoporous RuO_x

Fig. 6a,e shows the microscopic image of the bare electrode before electro-deposition. The black portion is the carbon electrode, and the white region is the electrode gap (glass substrate). Initial attempts to electro-deposit mesoporous Ru onto both electrodes 1 and 2 simultaneously (Scheme 1a) were unsuccessful. Deposition of active material in the electrode gap could not be avoided (Fig. 6b,f), leading to electrical short-circuiting which could easily be confirmed by checking the resistance between electrodes 1 and 2. Sequential electro-deposition onto electrode 1 followed by electro-deposition onto electrode 2 also proved ineffective (Scheme 1b, Fig. 6c,g). In order to evade deposition of electrode material within the 5 μm gap, sequential electro-deposition using a reverse bias was conducted using a bi-potentiostat system as shown in Scheme 1c. Mesoporous Ru was first electro-deposited by applying −0.3 V vs. Ag/AgCl to electrode 1 for 15 min while keeping the potential of electrode 2 at 1.0 V vs. Ag/AgCl. The potential of electrode 2 is essential to assure that electrodes 1 and 2 are not short-circuited. Next, the potentials of the two working electrodes were reversed to electro-deposit mesoporous Ru metal onto electrode 2. This sequence was repeated 3 times. As shown in Fig. 6b,f, preferential electro-deposition onto both electrodes 1 and 2 was achieved by this bi-potentiostatic deposition technique.

The microscopic image of the bare IDA electrode is compared with that after the first bi-potentiostatic electro-deposition onto electrode 1 in Fig. 7a and b. Three regions with different contrast could be observed after the first bi-potentiostatic electro-deposition (Fig. 7b). The black region is the bare carbon electrode 2, the gray region is electrode 1 with electro-deposited mesoporous Ru metal, and the white area is the glass substrate. It should be noted that such clear images could not be obtained without the reverse bias. The microscopic image of the IDA after 3 cycles of bi-potentiostatic electro-deposition onto electrodes 1 and 2 is shown

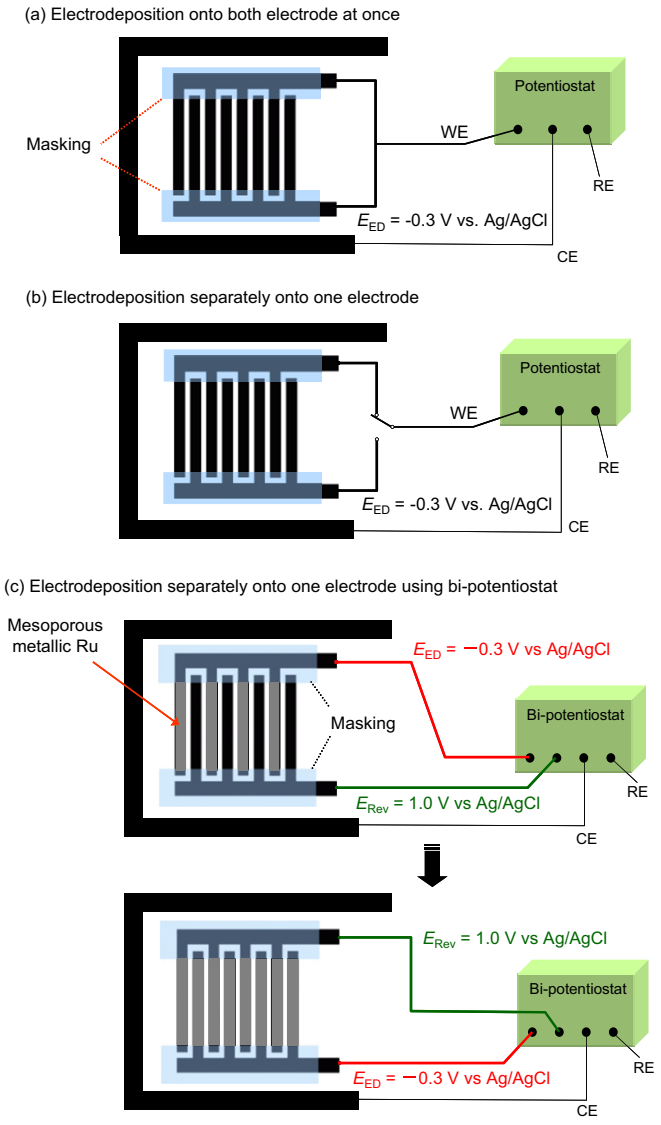

Scheme 1. Schematic of electro-deposition procedure of mesoporous Ru metal onto IDA electrode. (a) Electro-deposition onto both electrodes at once, (b) sequential electro-deposition onto one electrode at a time, and (c) bi-potentiostatic electro-deposition onto one electrode at a time.

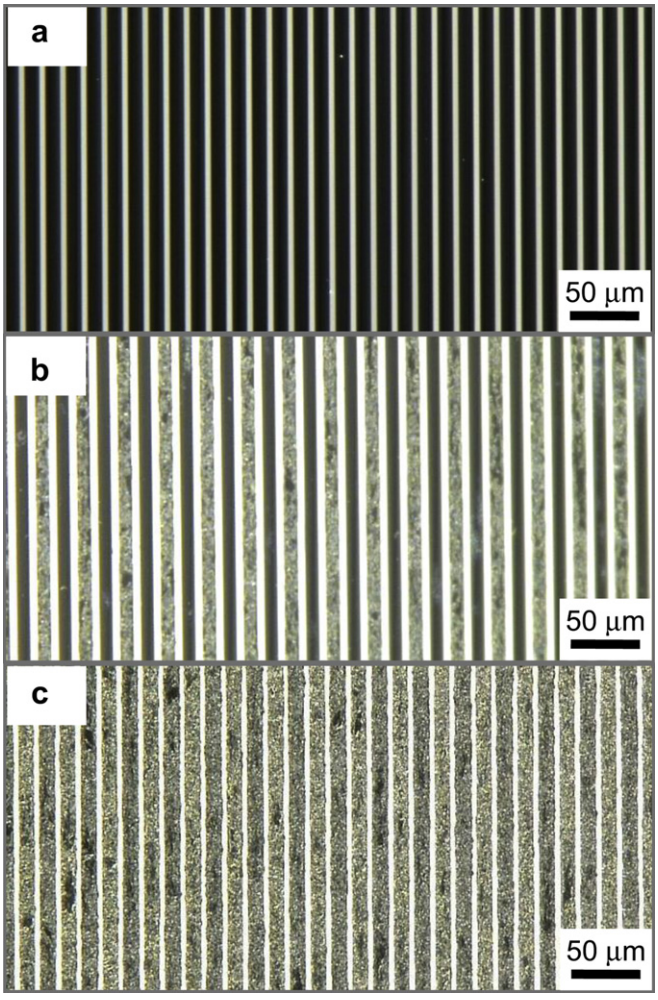

Fig. 7. Optical microscopic images of IDA electrode for (a) before electro-deposition, (b) after bi-potentiostatic electro-deposition onto one side, (c) after bi-potentiostatic electro-deposition onto both electrodes.

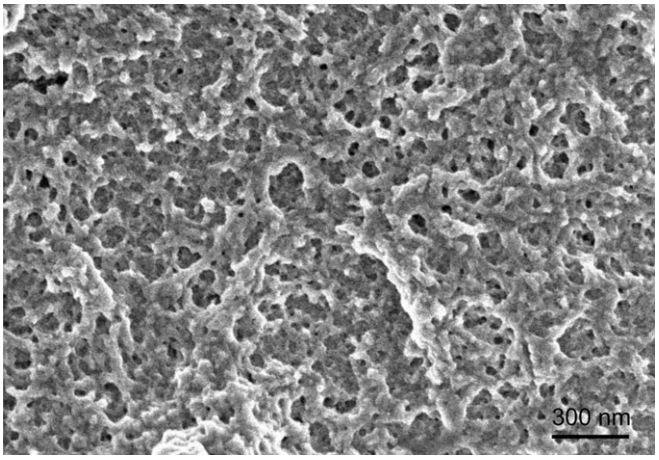

Fig. 8. SEM image of mesoporous Ru metal/IDA electrode.

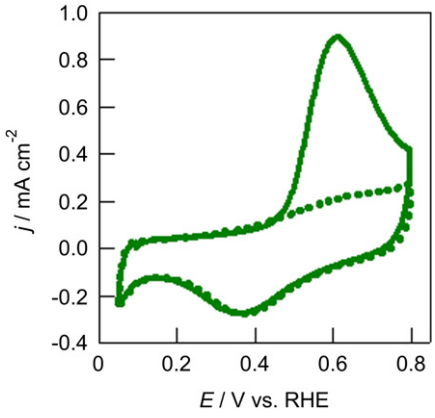

Fig. 9. CO-stripping voltammogram of mesoporous Ru metal on IDA electrode for electrode 1 + 2 (electrodes 1 and 2 connected in series) in 0.5 M H_2SO_4 at 2 mV s^{-1}.

in Fig. 7c. No short-circuiting was observed. SEM images of the electro-deposited Ru showed wormhole-like mesostructure (Fig. 8).

CO-stripping voltammograms of mesoporous Ru metal on IDA electrode for electrode 1 + 2 are exhibited in Fig. 9. The calculated surface area of Ru metal on IDA electrode is 40.3 cm^2. Based on the

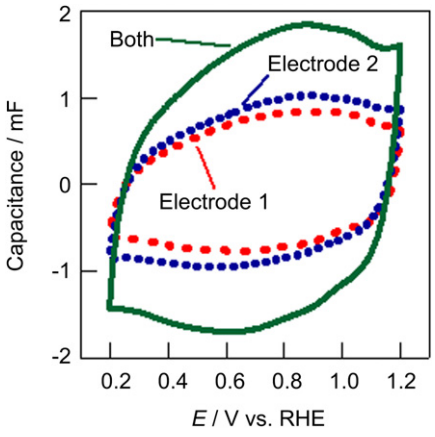

Fig. 10. Cyclic voltammograms of mesoporous RuO_x/IDA electrode for electrodes 1, 2 and electrode 1 + 2 (electrodes 1 and 2 connected in series) both at 50 mV s^{-1} in 0.5 M H_2SO_4.

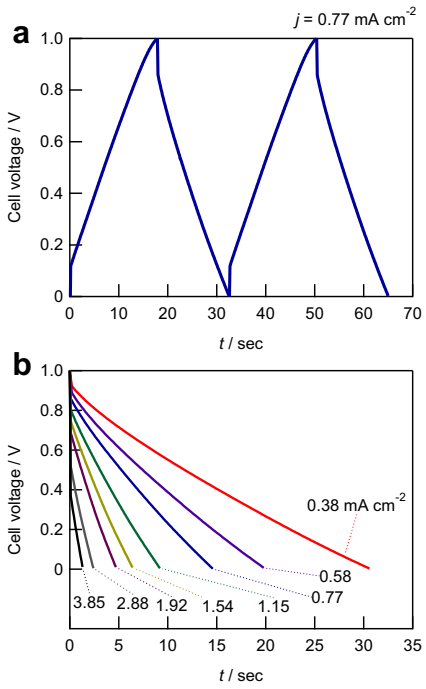

Fig. 11. (a) Charge/discharge curve at 0.77 mA cm^{-2} and (b) discharge curves at various discharge currents for mesoporous RuO_x micro-supercapacitor in 0.5 M H_2SO_4.

specific surface area of mesoporous Ru metal/Ti of 130 m^2 g^{-1} (E_{ED} = −0.3 V vs. Ag/AgCl), the amount of Ru on Ru/IDA is estimated as 3.1 μg (119 μg cm^{-2}).

Mesoporous Ru/IDA electrode was converted to mesoporous RuO_x/IDA by electro-oxidation in 0.5 M H_2SO_4. Cyclic voltammograms of mesoporous RuO_x/IDA for electrodes 1 and 2 measured individually in a three-electrode system are shown in Fig. 10. The capacitance of electrodes 1 and 2 was 0.604 mF and 0.732 mF, respectively. It can thus be said that the electro-deposited amount of mesoporous RuO_x onto both electrodes was similar. If electrodes 1 and 2 were to be short-circuited, the capacitance of electrode 1, electrode 2, and electrode 1 + 2 (electrodes 1 and 2 connected in series) would all be equal. The capacitance of electrode 1 + 2 gave capacitance of 1.328 mF (Fig. 10), matching the sum of the capacitance of electrodes 1 and 2. Using the capacitance of 1.328 mF and the specific capacitance value of 380 F (g-Ru)$^{-1}$ for mesoporous Ru metal/Ti (E_{ED} = −0.3 V vs. Ag/AgCl), the amount of Ru on Ru/IDA is estimated as 3.49 μg. The estimated value is in good agreement with that obtained from CO-stripping voltammetry.

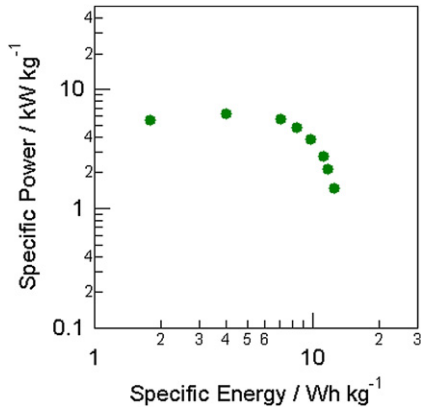

Fig. 12. Ragone plot of fabricated mesoporous RuO_x micro-supercapacitor.

The capacitive performances of mesoporous RuO_x/IDA micro-supercapacitor were measured by constant-current charge/discharge measurements. Constant current charge/discharge curves after electro-oxidation of mesoporous Ru exhibited ideal capacitive charge/discharge behavior as given in Fig. 11a. At the smallest current density of 0.38 mA cm^{-2}, a maximum specific capacitance of 12.6 mF cm^{-2} (0.328 mF) was obtained. The capacitance value of 0.328 mF is approximately one-half of the single electrode capacitance of electrode 1 (0.604 mF) obtained from cyclic voltammetry. This is in agreement to the capacitance equation of a two electrode system where $C_{two} = 1/C_{electrode\ 1} + 1/C_{electrode\ 2}$.

The specific capacitance, energy, and power were calculated using the mass of Ru obtained from CO-stripping voltammetry (3.1 μg-Ru). The maximum specific energy was 12.5 Wh (kg-Ru)$^{-1}$ (1.49 μWh cm^{-2}) at 0.38 mA cm^{-2} and maximum specific power was 6.29 kW (kg-Ru)$^{-1}$ (750 μW cm^{-2}) at 2.88 mA cm^{-2} (Fig. 12, Table S1). The energy density is comparable to a RuO_2-based micro-supercapacitor fabricated by laser direct write and micromachining [15]. The obtained power performance is not as good as expected, maybe due to ohmic resistance of the carbon-based IDA electrode.

4. Conclusion

We have successfully prepared ordered mesoporous Ru metal thin film on a Ti substrate by electro-deposition process from lyotropic liquid crystal as a template. The ordered mesoporous Ru metal has a well-ordered mesoporous structure in a hexagonal array with electrochemically active surface area of ~100 m^2 g^{-1}. Hexagonally ordered mesoporous RuO_x/Ti was obtained by electro-oxidation in 0.5 M H_2SO_4 and exhibited a specific capacitance of ~400 F (g-Ru)$^{-1}$. Furthermore, mesoporous RuO_x was successfully electro-deposited onto an IDA electrode composed of a pair of 65 electrodes with 10 μm width and 5 μm gap. Mesoporous Ru metal was electro-deposited onto the IDA electrode using bi-potentiostatic electro-deposition and subsequently electro-oxidized. The thus prepared mesoporous RuO_x micro-supercapacitor exhibited good electrochemical capacitor properties with specific capacitance of 12.6 mF cm^{-2} and a specific energy of 12.5 Wh (kg-Ru)$^{-1}$.

Acknowledgments

This work was supported in part by a Grant-in-Aid for Global COE Program from the Ministry of Education, Science, Sports, and Culture (MEXT). One of the authors (W. Sugimoto) thanks Amano Institute of Technology for financial support.

Appendix A. Supplementary material

Supplementary material associated with this article can be found, in the online version, at http://dx.doi.org/10.1016/j.jpowsour.2012.11.032.

References

[1] C.K. Fredrikson, Z.H. Fan, Lab Chip 4 (2004) 526–533.
[2] N. Minc, J.-L. Viovy, C. R. Phys. 5 (2004) 565–575.
[3] S. Motokawa, M. Mohamedi, T. Momma, S. Shoji, T. Osaka, Electrochem. Commun. 6 (2004) 562–565.
[4] J.R. Miller, A.F. Burke, Electrochem. Soc. Interf. 17 (2008) 53–57.
[5] J.-H. Sung, S.-J. Kim, K.-H. Lee, J. Power Sources 124 (2003) 343–350.
[6] J.-H. Sung, S.-J. Kim, S.-H. Jeong, E.-H. Kim, K.-H. Lee, J. Power Sources 162 (2006) 1467–1470.
[7] W. Sun, X. Chen, Microelectron. Eng. 86 (2008) 1307–1310.
[8] W. Sun, R. Zheng, X. Chen, J. Power Sources 195 (2010) 7120–7125.
[9] D. Pech, M. Brunet, P.-L. Taberna, P. Simon, N. Fabre, F. Mesnilgrente, V. Conéeéra, H. Durou, J. Power Sources 195 (2010) 1266–1269.
[10] D. Pech, M. Brunet, H. Durou, P. Huang, V. Mochalin, Y. Gogotsi, P.-L. Teberna, P. Simon, Nat. Nanotechnol. 5 (2010) 651–654.
[11] C. Shen, X. Wang, W. Zhang, F. Kang, J. Power Sources 196 (2011) 10465–10471.
[12] M. Beidaghi, W. Chen, C. Wang, J. Power Sources 196 (2011) 2403–2409.
[13] H.J. In, S. Kumar, Y. Shao-Horn, G. Barbastathis, Appl. Phys. Lett. 88 (2006) 083104-1–083104-3.
[14] J.P. Zheng, P.J. Cygan, T.R. Jow, J. Electrochem. Soc. 142 (1995) 2699–2703.
[15] C.B. Arnold, R. Wartena, K.E. Swider-Lyons, A. Pique, J. Electrochem. Soc. 150 (2003) A571–A575.
[16] G.S. Attard, P.N. Bartlett, N.R.B. Coleman, J.M. Elliott, J.R. Owen, J.H. Wang, Science 278 (1997) 838–840.
[17] G.S. Attard, C.G. Goltner, J.M. Corker, S. Henke, R.H. Templer, Angew. Chem. Int. Ed. Engl. 36 (1997) 1315–1317.
[18] Y. Yamauchi, T. Momma, M. Fuziwara, S.S. Nair, T. Ohsuna, O. Terasaki, T. Osaka, K. Kuroda, Chem. Mater. 17 (2005) 6342–6348.
[19] Y. Yamauchi, A. Sugiyama, R. Morimoto, A. Takai, K. Kuroda, Angew. Chem. Int. Ed. 47 (2008) 5371–5373.
[20] P.A. Nelson, J.M. Elliott, G.S. Attard, J.R. Owen, Chem. Mater. 14 (2002) 524–529.
[21] Y. Yamauchi, T. Momma, T. Yokoshima, K. Kuroda, T. Osaka, J. Mater. Chem. 15 (2005) 1987–1994.
[22] A. Takai, T. Saida, W. Sugimoto, L. Wang, Y. Yusuke, K. Kuroda, Chem. Mater. 21 (2009) 3414–3423.
[23] D. Zhao, W. Zhou, H. Li, Chem. Mater. 19 (2007) 2882–3891.
[24] D.-D. Zhao, M.W. Xu, W.-J. Zhou, J. Zhang, H.L. Li, Electrochim. Acta 53 (2008) 2699–2705.
[25] W. Sugimoto, S. Makino, R. Mukai, Y. Tatsumi, K. Fukuda, Y. Takasu, Y. Yamauchi, J. Power Sources 204 (2012) 244–248.
[26] T. Kawaguchi, W. Sugimoto, Y. Takasu, Electrochemistry 78 (2010) 36–41.